Chapter 4

Control of magnetotactic bacteria

Islam S.M. Khalil*, Sarthak Misra†
*The German University in Cairo, New Cairo City, Egypt
†University of Twente, Enschede, The Netherlands

CHAPTER OUTLINE

4.1 INTRODUCTION

Over the past decade, man-made robots at the nano- and micro-scales have shown potential to revolutionize medicine by reaching regions inaccessible to catheterization. They can be powerful enough to push or pull payloads to previously inaccessible body locations. Since 2001, when the first self-propelled object was built by Ismagilov et al. [1], the field of nano- and micro-robotics has passed quickly through several stages from understanding and development of locomotion mechanisms to the control of nano-motors inside living human cells by Wang et al. [2]. Nelson et al. presented an excellent survey on that subject [3] with focus on the locomotion mechanisms of microrobot, powering, and visualization of microrobotic systems using clinical imaging modalities. In this chapter, the focus is on magnetotactic bacteria (MTBs) that have been discovered by Blakemore four decades ago [4,5]. These microorganisms have full autonomous motion that allows them to be used in diverse biomedical applications using external magnetic fields. Characterization and control of these magnetic microorganisms are addressed in this chapter.

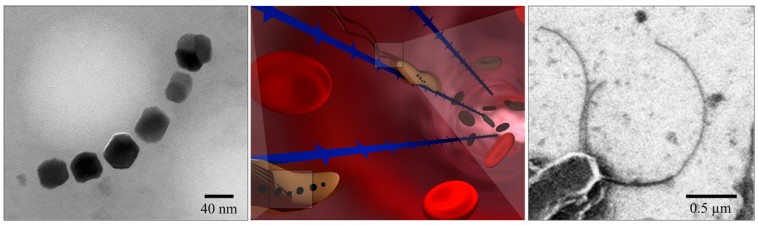

■ **FIGURE 4.1** Conceptual image of magnetotactic bacteria (MTBs) steered under the influence of external magnetic fields in a blood vessel. MTBs align themselves along the magnetic field lines (blue lines [dark gray in print version]) and move by rotating their helical flagella. The alignment is achieved using magnetite (Fe_3O_4) nano-crystals that are contained inside the cell.

MTBs can controllably navigate throughout the human circulatory system and reach deep-seated regions (Fig. 4.1). Their size, magnetic properties, and motility enable high precision motion control using an external magnetic field *only* for directional control. The flagellated swim of MTBs allows researchers to use weak magnetic field (millitesla range) for steering without relatively large magnetic field gradient. Martel et al. have demonstrated the directional control of swarm of MTBs (magnetotactic coccus strain MC-1) and single bacterium [6]. In addition, this strain has been used to achieve micro-actuation [7] and micro-assembly [8,9] of non-magnetic beads and objects, respectively. Khalil et al. have also demonstrated open- and closed-loop control of MTBs (*Magnetospirillum Magnetotacticum* Strain MS-1 and *M. magneticum* Strain AMB-1) inside capillary tube and microfluidic channels with structure of a maze [10,11]. In addition, a comparative study between MTBs (Fig. 4.2) and self-propelled microjets has proven that MTBs are more efficient and swim at approximately 3 times the body-length-per-second of the self-propelled microjets [12,13]. Kim et al. have also demonstrated control of *Tetrahymena Pyriformis* cells in three-dimensional space using two sets of Helmholtz coils and single electromagnet to control the planar and vertical motion of these cells, respectively [14]. A null-space control has also been proposed in [15], and the accuracy of the motion control has been increased by projecting an additional control input onto the null space of the magnetic force–current map of the electromagnetic system. The projection of this additional control input enables oscillation of the magnetic fields and directional control towards a reference position to decrease the speed of the MTB within the vicinity of the reference position. Although the null-space control strategy decreases the region-of-convergence of the controlled MTB within the vicinity of the reference position, the generation of oscillating magnetic fields may have adverse effects on the electromagnetic coils. The alternating current causes the coils to heat up and decreases their availability, for instance. Hassan et al.

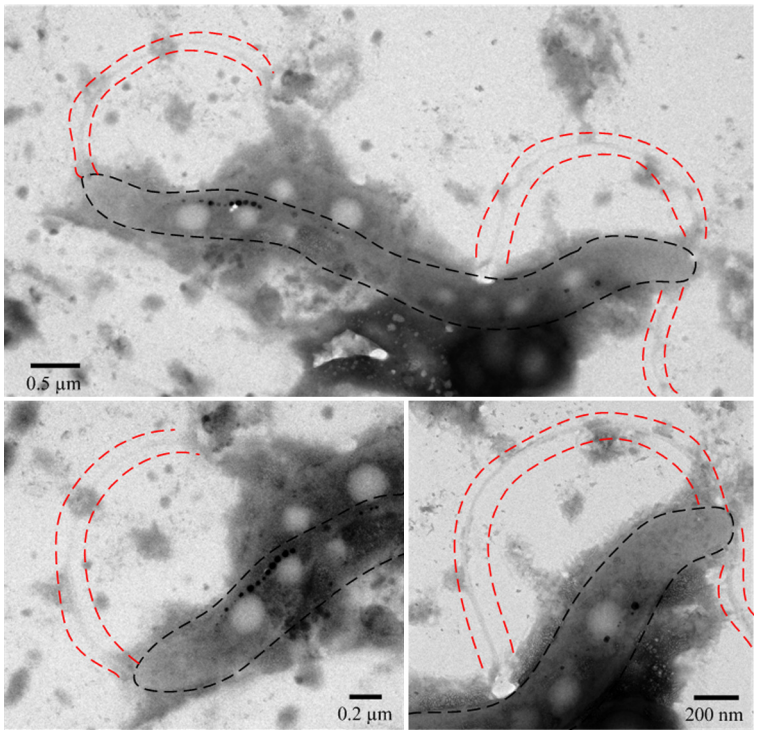

■ **FIGURE 4.2** Scanning Electron Microscopy images of magnetotactic bacteria (*Magnetospirillum Magnetotacticum* Strain MS-1). The black and red (mid gray in print version) dashed lines indicate the cell of the bacterium and its flagella, respectively.

have proposed an adaptive control strategy that allows the magnetic field to increase with the decreasing position error between the MTB and the reference position [16]. This control strategy has achieved accurate positioning of the motile MTBs with position error of less than a body-length. It has also been demonstrated that the positioning accuracy is mainly affected by the magnetic properties of the MTBs [17]. An MTB with greater magnetic dipole moment undergoes faster *U-turn* trajectories under the influence of magnetic field reversals, and hence an MTB with greater dipole can be positioned with higher accuracy, for instance.

4.2 CHARACTERIZATION OF MAGNETOTACTIC BACTERIA

Characterization of magnetotactic bacteria includes Scanning Electron Microscopy (SEM) imaging of the cells to determine their morphology

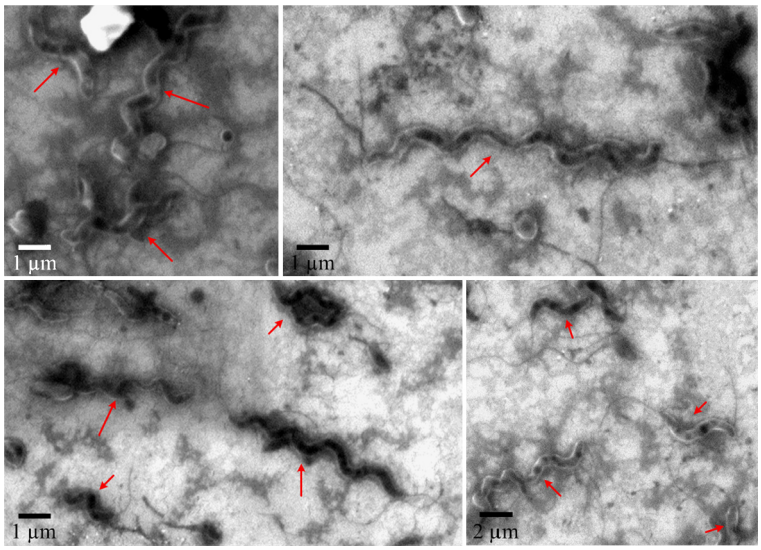

■ **FIGURE 4.3** Scanning Electron Microscopy images of magnetotactic bacteria (*M. magneticum* Strain AMB-1). The red (mid gray in print version) arrows indicate the cell of the bacterium.

(Fig. 4.3) and the shape and size of the magnetite (Fe_3O_4) nano-crystals that are contained inside the cell, as shown in Fig. 4.2. Transmission Electron Microscopy (TEM) images are also essential to determine the length and thickness of the flagella. The magnetotactic bacterial strains are *Magnetospirillum magnetotacticum* (ATCC 31632) and *M. magneticum* (ATCC 700264). The *Magnetospirillum magnetotacticum* and *M. magneticum* cells are incubated in MSGM mediums (ATCC 1653) with oxygen concentration of approximately 1% [18]. The cultures are incubated at 30°C for 4 to 10 days. Cells are harvested when a small gray sediments are visible at the bottom of the tubes. The growth conditions of the magnetotactic bacteria affect their characteristics, and different magnetic properties can be achieved based on these conditions [19].

SEM and TEM images are taken from the same cultures of the mentioned bacterial strains and their morphology is summarized in Table 4.1. The SEM images in Figs. 4.2 and 4.3 show that these MTBs possess flagella (indicated using the red dashed lines) at both sides. The MTB swims by wrapping its flagella together in a helical bundle, and the continuous rotation of this bundle enables locomotion and swimming back-and-forth. The locomotion of an MTB (*Magnetospirillum Magnetotacticum* Strain MS-1) is shown in Fig. 4.4. The MTB rotates its helical bundle and also rotates its helical body like a corkscrew (Fig. 4.3). An external source of magnetic field enables

Table 4.1 Morphology of the *Magnetospirillum magnetotacticum* and *M. magneticum* strains: The characteristics are calculated from 15 Scanning and Transmission Electron Microscopy images of each bacterial strain. These results are based on the recommended growth condition of the two bacterial strains

Characteristics	***Magnetospirillum magnetotacticum***	***M. magneticum***
Cell length (l) [μm]	5.2 ± 0.5	2.5 ± 0.6
Cell diameter (d) [μm]	0.5 ± 0.1	0.4 ± 0.1
Flagellum length [μm]	12 ± 3	7 ± 2
Flagellum thickness [nm]	~20	~20
Nano-crystals morphology	cuboctahedral	cuboctahedral
Nano-crystals edge length [nm]	30 ± 8	29 ± 13
Number of nano-crystals	18 ± 5	15 ± 7

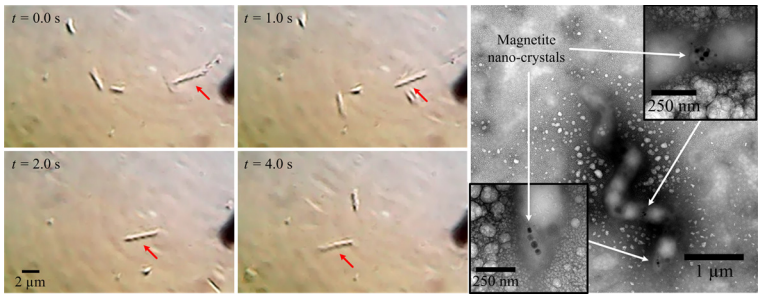

■ **FIGURE 4.4** Magnetotactic bacterium (*Magnetospirillum Magnetotacticum* Strain MS-1) swims by rotating its helical flagella and also by rotating its helical body like corkscrew (red arrows [mid gray in print version]). The helical morphology of the cell is shown by the Scanning Electron Microscopy image, and the white arrows indicate the magnetite nano-crystals.

directional control by exerting a magnetic torque on the nano-crystals of the MTB, as shown in the SEM image in (Fig. 4.4). In order to calculate this magnetic torque, we characterize the magnetic dipole moment of these nano-crystals. The magnetic dipole moment can be characterized from the SEM or TEM images of the MTBs. The total volume of the magnetite nano-crystals is deduced from the TEM images of the cells, and used in the calculation of their magnetic dipole moments. The magnetic dipole moment ($\mathbf{m}$) has an upper limit that is given by

$$|\mathbf{m}| = \sigma \sum_{j=1}^{k} \mathrm{m}_j, \tag{4.1}$$

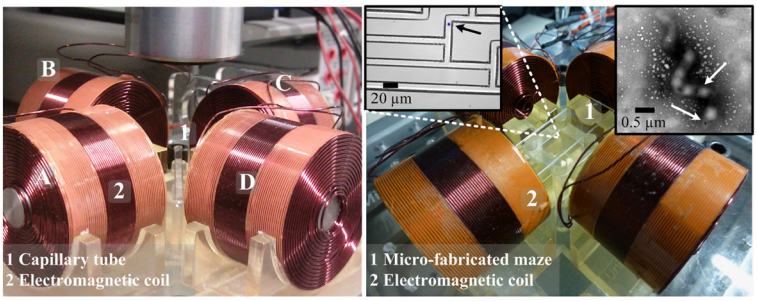

■ **FIGURE 4.5** An electromagnetic system for the characterization and control of magnetotactic bacteria inside capillary tubes (left) and microfluidic channel with a maze structure (right).

where σ is the saturation magnetization of magnetite (60 A m^2/kg) [20]. Further, k and m_j are the number and volume of the jth magnetite nanocrystal, respectively. Using (4.1), the upper limits of the magnetic dipole moments are calculated to be 2.9×10^{-16} A m^2 and 2.1×10^{-16} A m^2 for the *Magnetospirillum magnetotacticum* and *M. magneticum* cells, respectively. Bahaj et al. [21,22] and Steinberger et al. [23] have proposed motion analysis-based techniques (*U-turn*, *rotating-field*, and *flip-time*) to determine the magnetic dipole moment of motile and non-motile MTBs. These techniques are based on the control of the magnetic field lines. Fig. 4.5 shows an electromagnetic system with 4 electromagnetic coils in an orthogonal configuration. This setup enables directional control of the magnetic field lines. The *U-turn* and *flip-time* experiments can be done using single electromagnetic coil to provide field reversals, whereas the *rotating-field* experiment is based on 2 electromagnetic coils to provide rotating magnetic field at different frequencies. The electromagnetic coils surround a capillary tube (depth of 200 μm) or a microfluidic channel (depth of 5 μm). The far- and near-surface effects on the motion of the MTBs are studied using the capillary tube and microfluidic channel.

An MTB follows *U-turn* trajectories under the reversal of the magnetic fields. The *U-turn* diameter is given by

$$D = \frac{\alpha \pi v}{|\mathbf{m}||\mathbf{B}(\mathbf{P})|}, \tag{4.2}$$

where D is the diameter of the *U-turn*. The *U-turn* time is

$$\tau = \frac{\alpha}{|\mathbf{m}||\mathbf{B}(\mathbf{P})|} \ln\left(\frac{2|\mathbf{m}||\mathbf{B}(\mathbf{P})|}{\mathrm{k}T}\right), \tag{4.3}$$

where τ is the time of the *U-turn*. Further, k and T are the Boltzmann constant and the temperature of the fluid, respectively. Using (4.2) and (4.3),

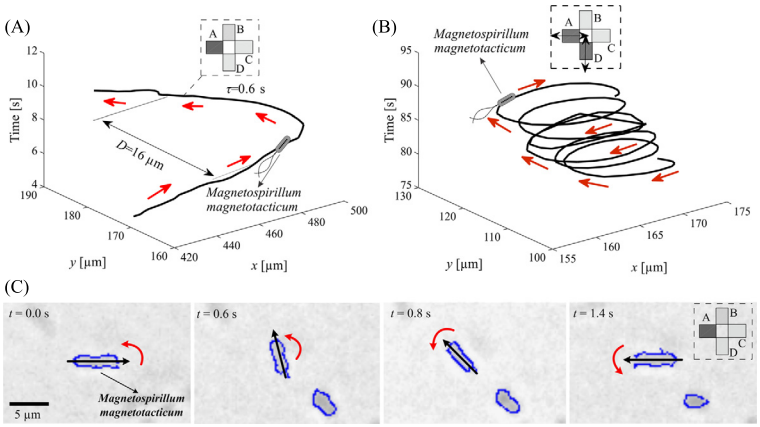

■ **FIGURE 4.6** Characterization of the magnetization of motile and non-motile magnetotactic bacteria (MTBs) using motion analysis-based techniques: (A) *U-turn* technique is based on applying magnetic field reversals and calculating the diameter of the *U-turn* trajectory. (B) Rotating field technique is based on applying rotating field and the determination of the boundary frequency. (C) Flip-time technique is used to calculate the magnetization of non-motile MTBs.

we calculate the magnetic dipole moment for each strain. Therefore, we determine the diameter and the time of the *U-turn* trajectory of the MTB, as shown in Fig. 4.6(A).

Under the influence of a rotating magnetic field, a motile MTB follows circular trajectories (Fig. 4.6(B)). The angular velocity of the cells increases by increasing the frequency of the rotating magnetic fields. The cells follow circular trajectories up to a frequency, i.e., boundary frequency (ω_b), after which the cell can no longer follow the rotating fields. We assume that the torque (Ω) generated by the helical flagella can be ignored [24]. Therefore, the relation between the magnetic torque and the angular velocity of the cell (ω) is given by

$$|\mathbf{m}|\,|\mathbf{B}(\mathbf{P})|\sin\beta + \alpha\omega = 0, \tag{4.4}$$

where β is the angle between the induced magnetic field and the magnetic dipole moment of the MTB. Characterization of the magnetic dipole moment requires the determination of its boundary frequency (ω_b). This frequency can be determined by gradually increasing the frequency of the rotating field and observing the frequency after which the cell can no longer follow the rotating magnetic fields, i.e., $\omega = \omega_b$, when $\sin\beta = 1$. Therefore, (4.4) can be written as

$$|\mathbf{m}|\,|\mathbf{B}(\mathbf{P})| + \alpha\omega_b = 0. \tag{4.5}$$

Table 4.2 Characterized magnetic dipole moment of the *Magnetospirillum magnetotacticum* strain MS-1 and *M. magneticum* strain AMB-1 using the *U-turn* technique, the *rotating-field* technique, and the *flip-time* technique. The averages are calculated from 10 characterization experiments for each bacterial strain

Characteristics	*Magnetospirillum magnetotacticum*	*M. magneticum*
U-turn diameter (D) [μm]	16 ± 3.1	8.9 ± 1.8
U-turn time (τ) [s]	0.6 ± 0.2	0.7 ± 0.3
Dipole moment ($\|\mathbf{m}\|$) [A m^2]	1.6×10^{-16}	1.5×10^{-17}
Boundary frequency (ω_b) [rad/s]	9.5 ± 1.7	8.1 ± 2.6
Dipole moment ($\|\mathbf{m}\|$) [A m^2]	1.3×10^{-16}	1.5×10^{-17}
Flip-time (τ) [s]	1.4 ± 0.7	2.7 ± 0.8
Dipole moment ($\|\mathbf{m}\|$) [A m^2]	0.5×10^{-16}	0.1×10^{-17}

Finally, during magnetic field reversals, non-motile magnetotactic bacteria exhibit flip turns. The *flip-time* of each turn can be determined from the motion analysis of the cells. The *flip-time* is given by (4.3) and is shown in Fig. 4.6(C). Table 4.2 provides a comparison between the characterized magnetic dipole moment of the *Magnetospirillum magnetotacticum* strain MS-1 and *M. magneticum* strain AMB-1 using the motion analysis-based techniques.

Eqs. (4.2), (4.3), and (4.4) indicate the influence of the magnitude of the magnetic field on the *U-turn* diameter, elapsed time of the *U-turn* trajectory, and the boundary frequency of the MTB. Fig. 4.7 demonstrates the influence of the magnetic field on the diameter of the *U-turn* trajectory of the same MTB. The magnetic field is increased from 4.1 to 8.3 mT during the magnetic field reversals and the corresponding *U-turn* diameters are calculated to be 19 and 7 μm, respectively. Therefore, under the influence of magnetic field reversal with approximately twice the field strength, the diameter of the *U-turn* trajectories taken by the magnetotactic bacteria is decreased by 63%. This observation allows us to adjust the diameter and elapsed-time of the *U-turn* trajectories taken by an MTB. Localization of an MTB can be achieved within the vicinity of a reference position, as shown in Fig. 4.8. The vertical black line represents a reference position. The MTB is localized within its vicinity by multiple reversals of the magnetic field lines. Once the MTB is within the vicinity of the reference position, the magnetic field is measured to be 1.0 mT. At time $t = 12$ s, the magnitude of the magnetic field is in-

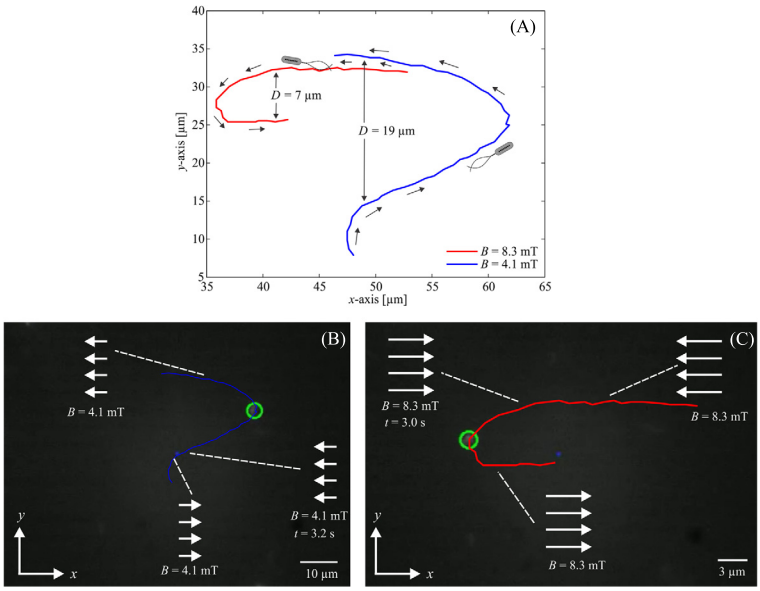

■ **FIGURE 4.7** A representative *U-turn* experiment of a magnetotactic bacterium (MTB), i.e., *Magnetospirillum gryphiswaldense* strain MSR-1, under the influence of magnetic field reversals. This trial is done using the same MTB. The *U-turn* experiment is done at 2 magnetic fields, i.e., 4.1 mT and 8.3 mT. The green (gray in print version) circle indicates the MTB.

creased to 1.4 mT. This increase results in faster *U-turn* trajectories with smaller diameter. Therefore, the magnitude of the magnetic field influences the positioning accuracy and has to be varied to increase the accuracy of the positioning of an MTB.

4.3 CONTROL OF MAGNETOTACTIC BACTERIA

Microrobots can be categorized based on their locomotion mechanism [25] into magnetically-driven and self-driven microrobots (Fig. 4.9). The self-driven microrobots [26–28] benefit from the greater projection distance of the magnetic field, as opposed to the projection distance of the magnetic field gradient [3]. MTBs are self-propelled and have the following advantages over other self-propelled microrobots:

- In contrast to microrobotic system that are powered and steered using bubble propulsion [26], MTBs are biocompatible and suitable for nanomedicine and biomedical application;
- The size of the MTBs enables them to navigate through the smallest capillaries of the human body;

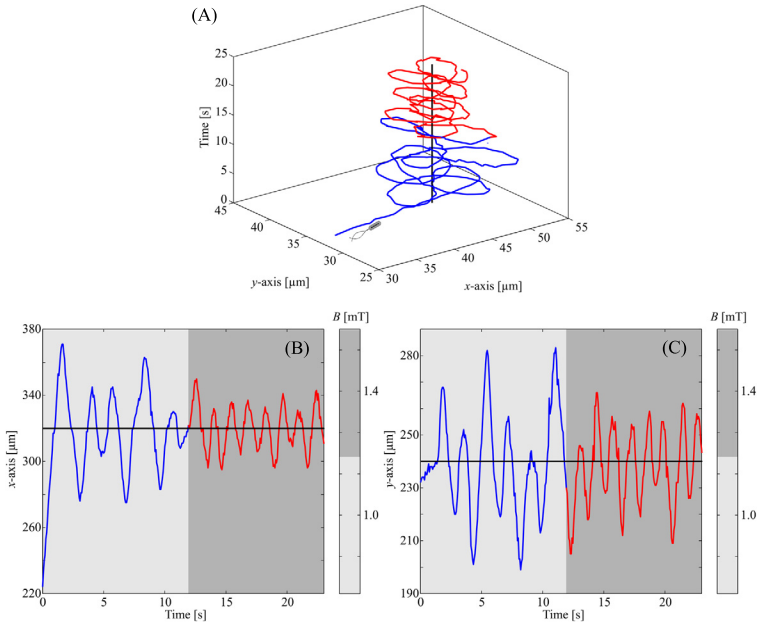

■ **FIGURE 4.8** The influence of the magnitude of the magnetic field on the localization accuracy of a magnetotactic bacterium (MTB).

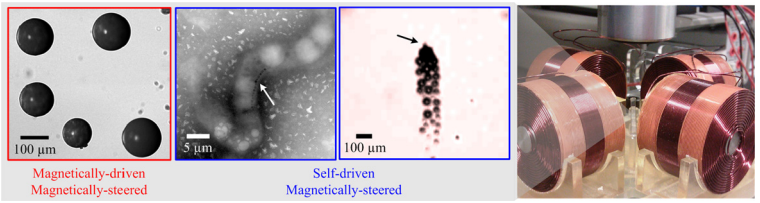

■ **FIGURE 4.9** Magnetically-driven and self-driven microrobots are controlled using external source of magnetic fields. Paramagnetic microparticles are magnetically-driven, whereas the magnetotactic bacteria and self-propelled microjets are self-propelled by the helical flagella and the ejection of oxygen bubbles, respectively.

- MTBs are magnetic and it is not necessary to embed a magnetic layer to enable directional control.

Therefore, it is essential to achieve high precision motion control of MTBs to show their potential in nano-medicine and nano-technology applications. Here, we review a few open- and closed-loop control strategies of MTBs.

The magnetic dipole of the MTB enables the cell to align along the magnetic field lines. Therefore, an open-loop control strategy is devised based on directing the magnetic fields towards a desired direction based on the

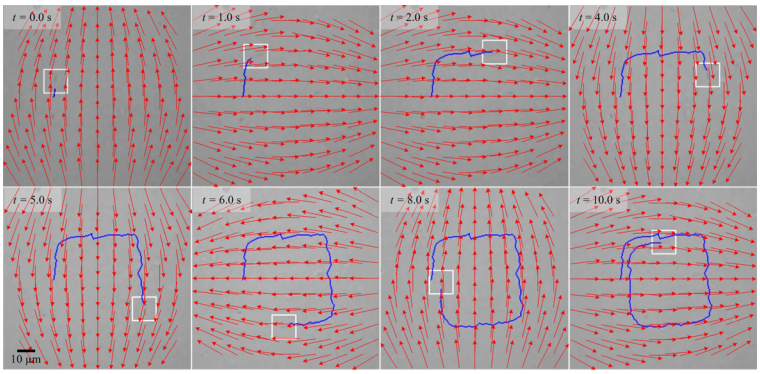

■ **FIGURE 4.10** A magnetotactic bacterium (MTB) swims along the magnetic field lines and achieves a square trajectory. The MTB is indicated using the white square, and the red (mid gray in print version) arrows represent the magnetic field lines.

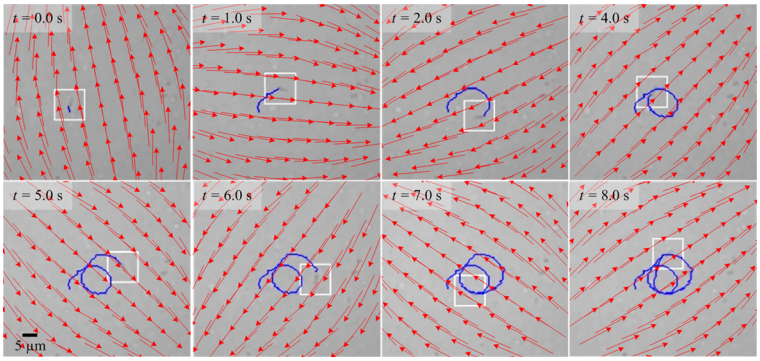

■ **FIGURE 4.11** A magnetotactic bacterium (MTB) swims along the magnetic field lines and achieves a circular trajectory. The MTB is indicated using the white square and the red (mid gray in print version) arrows represent the magnetic field lines.

position of the MTB. For example, directing the magnetic fields along 4 orthogonal directions enables a magnetic MTB to move along a square trajectory, as shown in Fig. 4.10. The MTB swims along the field lines at an average speed of 30 μm/s, and it changes its orientation based on the direction of the applied magnetic fields (red arrows). Fig. 4.11 shows an MTB under the influence of rotating magnetic fields. These fields are generated using two electromagnetic coils, and the MTB follows circular trajectories with diameter of 10 μm. More complex trajectories can be followed by the MTB using this open-loop control technique. However, closed-loop control system has to be designed to achieve accurate positioning of the MTBs.

The linear motion of an MTB in a fluid is approximated by

$$|\mathbf{F}(\mathbf{P})| + F_{\mathrm{d}} + f = 0, \tag{4.6}$$

where f is the propulsion force generated by the helical flagella, and F_{d} is the drag force on the MTB. We calculate the position and velocity tracking errors of the MTB with respect to a fixed reference position ($\mathbf{P_{ref}}$) as

$$\mathbf{e} = \mathbf{P} - \mathbf{P_{ref}} \text{ and } \dot{\mathbf{e}} = \dot{\mathbf{P}} - \dot{\mathbf{P}}_{\mathbf{ref}} = \dot{\mathbf{P}}, \tag{4.7}$$

where $\mathbf{e}$ and $\dot{\mathbf{e}}$ are the position and velocity tracking errors, respectively. We devise a desired magnetic force ($\mathbf{F_{des}}(\mathbf{P})$) of the form

$$\mathbf{F_{des}}(\mathbf{P}) = \mathbf{K_p}\mathbf{e} + \mathbf{K_d}\dot{\mathbf{e}}. \tag{4.8}$$

In (4.8), $\mathbf{K_p}$ and $\mathbf{K_d}$ are the controller positive-definite gain matrices, given by

$$\mathbf{K_p} = \begin{bmatrix} k_{\mathrm{p1}} & 0 \\ 0 & k_{\mathrm{p2}} \end{bmatrix} \text{ and } \mathbf{K_d} = \begin{bmatrix} k_{\mathrm{d1}} & 0 \\ 0 & k_{\mathrm{d2}} \end{bmatrix}, \tag{4.9}$$

where $k_{\mathrm{p}r}$ and $k_{\mathrm{d}r}$ $(r = 1, 2)$ are the proportional and derivative gains, respectively. Substituting (4.8) in the magnetic force equation (4.6), i.e., $\mathbf{F_{des}}(\mathbf{P}) = \mathbf{F}(\mathbf{P})$, and assuming no propulsion force ($f = 0$) yields the following position tracking error dynamics:

$$\dot{\mathbf{e}} + (\mathbf{K_d} + \gamma \mathbf{\Pi})^{-1} \mathbf{K_p}\mathbf{e} = 0, \tag{4.10}$$

where $\mathbf{\Pi}$ is the identity matrix and γ is the linear drag coefficient. Since $f \neq 0$, zero position tracking error cannot be achieved. However, the closed-loop control system positions the cell within the vicinity of the reference position, i.e., a region-of-convergence, based on (4.10). Therefore, the positioning accuracy of the closed-loop control system depends on the dynamic viscosity of the growth medium, morphology of the cells, the propulsion force of the flagella, and the controller gains. We evaluate the accuracy of the closed-loop control system using the size of the region-of-convergence.

Implementation of the closed-loop control law (4.8) is shown in Fig. 4.12. Two reference positions are provided and represented using the vertical blue lines (also indicated using ① and ②). The MTB swims towards the reference positions at an average speed of 30 μm/s, and the closed-loop control action localizes the MTB within their vicinities. The region-of-convergence of the first and second reference positions are calculated to be 55 μm and 30 μm in diameter, respectively. The region-of-convergence of the first reference position is twice greater than that of the second reference position

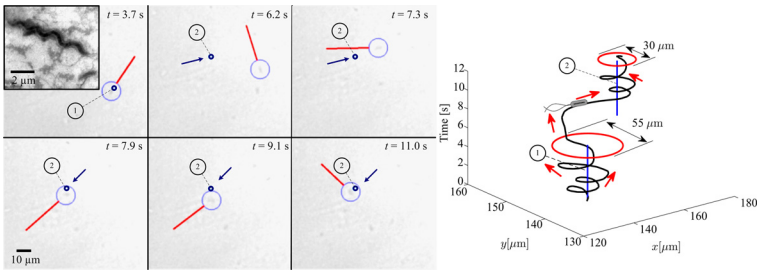

■ **FIGURE 4.12** A magnetotactic bacterium (MTB) swims towards two reference positions indicated using the small blue (dark gray in print version) circles. The MTB is indicated using the large blue (dark gray in print version) circle and its velocity vector is presented using the red (mid gray in print version) line. The MTB is indicated using the white square and the red (mid gray in print version) arrows represent the magnetic field lines. The MTB is controlled at an average velocity of 30 μm/s. The control system positions the MTB within the vicinity of two reference positions (vertical blue [dark gray in print version] lines) with regions of convergence of 55 μm and 30 μm in diameter.

using similar control gains (4.9). We attribute this behavior to the difference in the magnetic field magnitude between the positions ① and ②. The magnetic fields are not uniform throughout the workspace, and hence the positioning accuracy is influenced locally by the magnitude of the magnetic field. Fig. 4.8 shows that a slight increase of 0.4 mT in the magnitude of the magnetic field results in a decrease of the region-of-convergence. Hassan et al. have investigated the influence of the magnitude of the magnetic field on the behavior of *Magnetospirillum gryphiswaldense* strain MSR-1 [16]. It has been experimentally demonstrated that an adaptive magnetic field has to be provided to control the MTB throughout its path towards the reference position. It has been also suggested that the magnitude of the magnetic field has to be increased once the MTB reaches the reference position to increase the positioning accuracy. Fig. 4.13 demonstrates the influence of the magnetic field on the positioning accuracy of the MTBs. Each line represents the behavior of an MTB under the influence of different magnetic fields. The magnetic field is increased on the same bacterium (from the same culture), and we observe that higher magnetic field enables more accurate localization. This result also shows that the positioning accuracy is influenced by the properties of the MTBs. The blue (MTB_5) and yellow (MTB_6) lines in Fig. 4.13 represent control of 2 MTBs with region-of-convergence of less than a body-length, whereas the red (MTB_1) and green (MTB_2) lines represent control results of 2 other MTBs with region-of-convergence that is slightly greater than a body-length. Therefore, it is essential to implement adaptive control on MTBs with the greatest magnetic dipole moment.

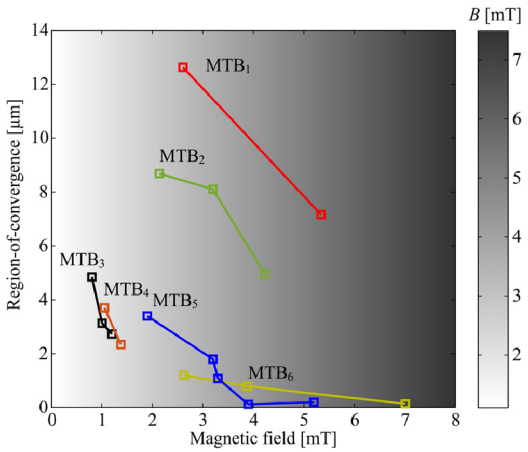

■ **FIGURE 4.13** Closed-loop control of magnetotactic bacteria (MTBs) at different magnetic fields is achieved [16]. Increasing the magnitude of the magnetic fields results in a decrease in the region-of-convergence of the controlled magnetotactic bacterium (MTB) and does not have an influence on its swimming speed. The 6 closed-loop control trials are done using MTBs from the same culture (*Magnetospirillum gryphiswaldense* strain MSR-1). Each trial is done using the same MTB.

Magnetotactic bacteria have the potential to controllably reach deep-seated regions of the body by vessels and achieve targeted drug delivery. In this application, motion of the magnetotactic bacteria is influenced by the near-surface effects such as the background flows and electrostatic interactions [29,30]. Khalil et al. [11] have implemented a qualitative study on the behavior of MTBs inside microfluidic channels with a maze structure, as shown in Fig. 4.14. Control system (4.8) allows the MTB to follow two reference positions indicated by the small blue circles. We observe that the MTB is positioned within the vicinity of the reference positions, and the region-of-convergence is 10 μm. The control system positions the MTB at a velocity of 8 μm/s. Table 4.3 provides a comparison between the characteristics of the controlled MTB outside and inside the micro-fabricated maze. The transient- and steady-states are analyzed by the speed of the MTB and the size of the region-of-convergence, respectively. The closed-loop control presented in this chapter shows that MTBs can be controlled regardless of far- and near-surface effects. Therefore, these microorganisms can be used in diverse biomedical applications such as nano-medicine and targeted drug delivery.

Magnetotactic bacteria can selectively target diseased cells and achieve targeted drug delivery. For instance, the size of human breast cancer cells (MCF-7) is 20 μm in average diameter (Figs. 4.2 and 4.3), whereas the aver-

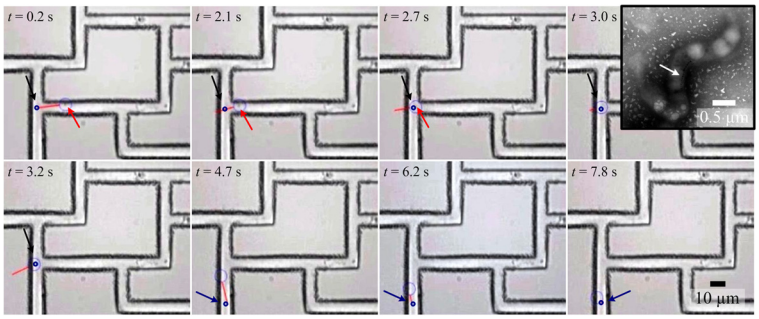

■ **FIGURE 4.14** Closed-loop control of a magnetotactic bacterium (MTB) inside a micro-fabricated maze with inner-width and -thickness of 10 and 5 μm, respectively, at various time (t) instants. This control system positions the MTB at a velocity of 8 μm/s and within a region-of-convergence of 10 μm. The black and blue (dark gray in print version) arrows indicate the first and second reference positions, respectively. The small blue (dark gray in print version) circles indicate these reference positions, whereas the large blue (light gray in print version) circle indicates the MTB. The red (light gray in print version) line represents the velocity vector of the MTB.

Table 4.3 Characteristics of the magnetotactic bacterium in the transient- and steady-states. Case I: Closed-loop control outside the micro-fabricated maze (inside a capillary tube). Case II: Closed-loop control inside the maze

Characteristics	Capillary tube	Maze
Speed (transient-state) [μm/s]	28	8
Region-of-convergence (steady-state) [μm]	18	10

age length and diameter of the MTBs are 5 and 0.5 μm, respectively. Therefore, the size of the magnetotactic bacteria enables selective targeting of these cells without affecting the healthy cells. Improving the positioning accuracy of MTBs is essential to targeting the diseased cells only. Wang et al. have demonstrated ultrasonic propulsion of gold nanomotors (nanomotors are propelled using ultrasonic waves and steered magnetically) inside HeLa cervical cancer cells [28]. The acoustic propulsion of these nanomotors allows them to remain active inside the cell and enables motion between cells (internalization of the nanomotors is achieved by incubation with the cells for longer than 24 hours). In contrast to gold nanomotors that are engulfed by the cells because of the long incubation period, magnetotactic bacteria are self-propelled, and accurate steering and positioning are achieved using magnetic field of millitesla range (Fig. 4.13). In addition, the aspect ratio of magnetotactic bacteria is high, and hence they are more prone to cell

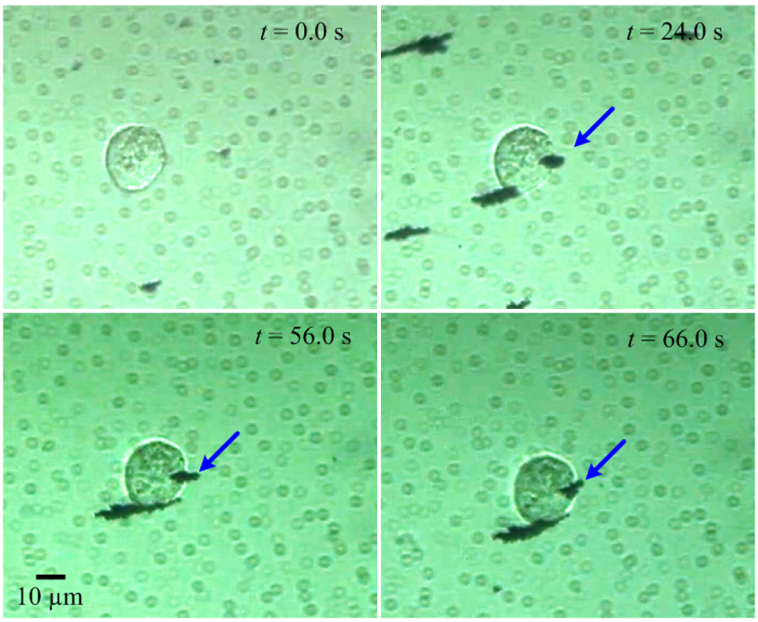

■ **FIGURE 4.15** Penetration of MCF-7 breast cancer cell using a cluster (bacterium mockup) of iron-oxide nano-particles (blue arrow) without causing damage to the cell membrane and without any effect on the cell morphology. The cluster and the magnetotactic bacterium (MTB) have similar aspect ratio (size of the cluster is twice the size of the MTB). Clusters with relatively large aspect ratio are more prone to cell uptake [31]. The cluster is pulled towards the cell using magnetic field and magnetic field gradient of 60 mT and 5 T/m, respectively. The cell uptake is achieved in approximately 1 minute without long incubation. MTBs have the potential to target cancer cells and penetrate the membrane without causing damage under the influence of directional control.

uptake than microorganisms with different morphologies. The cellular uptake of micro-particles has been studied by Gratton et al., and it has been demonstrated that micro-particles with high aspect ratios are more prone to cell uptake [31]. A preliminary experiment of cell uptake of a cluster of iron-oxide nano-particles (MTB mockup) is shown in Fig. 4.15. The aspect ratio of the cluster is adjusted to be similar to that of an MTB, whereas the size of the cluster is twice that of the MTB. This cluster is pulled under the influence of magnetic field gradient (magnetic gradient is 5 T/m and the magnetic force is measured to be less than 1 μN) towards an MCF-7 cell, and we observe immediate penetration after approximately 1 min [32]. MTBs can also be directed controllably towards the MCF-7 cells to achieve penetration or targeted drug delivery.

4.4 CONCLUDING REMARKS

In this chapter, we have presented culturing of MTBs, a family of characterization techniques of their magnetic properties and morphology, methods of open-loop and closed-loop control of MTBs, and a potential application of MTBs in nano-medicine. The culturing protocols of the MTBs [18] appear to be simple but they have a remarkable influence on the motility and magnetic properties of MTBs, as shown in Fig. 4.13. MTBs of the same culture possess different magnetic dipole (not all MTBs generate magnetite nano-crystals) and swim at difference speeds (MTBs has different number of flagella). The magnetic dipole moment has a far-reaching importance as we observe too many MTBs without nano-crystals, and hence they are not suitable for directional control. Lefevre et al. [19] have shown that the growth conditions of the magnetotactic bacteria affect their characteristics and different magnetic properties can be achieved based on these conditions. Nevertheless, properties of MTBs of the same culture show vast differences in magnetism and motility due to cell-to-cell variability. This issue has to be addressed extensively in future studies.

ACKNOWLEDGMENTS

The authors would like to thank Mr. Marc Pichel from the Korean Institute of Science and Technology for preparing the conceptual image in Fig. 4.1. They would also like to thank Ms. Heba A. Hassan and Mr. Tijmen Hageman from the Korean Institute of Science and Technology for collecting the data in Figs. 4.7, 4.6, and 4.13. Finally, they would also like to thank Prof. Leon Abelmann from the University of Twente and the Korean Institute of Science and Technology for many scientific discussions in all stages of the MTB project.

REFERENCES

[1] R.F. Ismagilov, A. Schwartz, N. Bowden, G.M. Whitesides, Angewandte Chemie International Edition 41 (2002) 652–654.
[2] W. Wang, S. Li, L. Mair, S. Ahmed, T.J. Huang, T.E. Mallouk, Angewandte Chemie 126 (2014) 3265–3268.
[3] B.J. Nelson, I.K. Kaliakatsos, J.J. Abbott, Annual Review of Biomedical Engineering 12 (2010) 55–85.
[4] R.P. Blakemore, Science 190 (1975) 377–379.
[5] R.P. Blakemore, R.B. Frankel, Scientific American 245 (1981) 58–65.
[6] S. Martel, O. Felfoul, J.-B. Mathieu, A. Chanu, S. Tamaz, M. Mohammadi, M. Mankiewicz, N. Tabatabaei, The International Journal of Robotics Research 28 (2009) 1169–1182.
[7] Z. Lu, S. Martel, Controlled bio-carriers based on magnetotactic bacteria, in: Proceedings of the IEEE International Conference on Solid-State Sensors, Actuators and Microsystems, Lyon, France, 2007, pp. 683–686.
[8] S. Martel, M. Mohammadi, Using a swarm of self-propelled natural microrobots in the form of flagellated bacteria to perform complex micro-assembly tasks, in: IEEE

International Conference in Robotics and Automation (ICRA), Alaska, USA, 2010, pp. 500–505.
[9] Z. Lu, S. Martel, Preliminary investigation of bio-carriers using magnetotactic bacteria, in: Proceedings of the IEEE Engineering in Medicine and Biology Society Annual International Conference (EMBS), New York City, USA, 2006, pp. 683–686.
[10] I.S.M. Khalil, M.P. Pichel, L. Zondervan, L. Abelmann, S. Misra, Characterization and control of biological microrobots, in: Proceedings of the 13th International Symposium on Experimental Robotics, Karlsruhe, Germany, in: Springer Tracts in Advanced Robotics, 2013, pp. 617–631.
[11] I.S.M. Khalil, M.P. Pichel, O.S. Sukas, L. Abelmann, S. Misra, Control of magnetotactic bacterium in a micro-fabricated maze, in: IEEE International Conference on Robotics and Automation, Karlsruhe, Germany, 2013, pp. 5488–5493.
[12] S. Sanchez, A.A. Solovev, S.M. Harazim, O.G. Schmidt, Journal of the American Chemical Society 133 (2010) 701–703.
[13] A.A. Solovev, S. Sanchez, M. Pumera, Y.F. Mei, O.G. Schmidt, Advanced Functional Materials 20 (2010) 2430–2435.
[14] D.H. Kim, P.S.S. Kim, A.A. Julius, M.J. Kim, Three-dimensional control of engineered motile cellular microrobots, in: IEEE International Conference on Robotics and Automation, Minnesota, USA, 2012, pp. 721–726.
[15] I.S.M. Khalil, M.P. Pichel, L. Abelmann, S. Misra, The International Journal of Robotics Research 32 (2013) 637–649.
[16] H.A. Hassan, M.P. Pichel, T. Hageman, L. Abelmann, I.S.M. Khalil, On the influence of the magnetic field strength on the control of *Magnetospirillum gryphiswaldense* strain MSR-1, in: Proceedings of the IEEE International Conference on Intelligent Robots and Systems (IROS), Daejeon, Korea, October 2016, pp. 5119–5124.
[17] I.S.M. Khalil, S. Misra, IEEE Transactions on Magnetics 50 (2014) 5000211.
[18] L.E. Bertani, J. Weko, K.V. Phillips, R.F. Gray, J.L. Kirschvink, International Journal on Genes and Genomes 264 (2001) 257–263.
[19] C.T. Lefevre, T. Song, J.-P. Yonnet, L.-F. Wu, Applied and Environmental Microbiology 75 (2009) 3835–3841.
[20] R.L. Rebodos, P.J. Vikesland, Langmuir 26 (2010) 16745–16753.
[21] A.S. Bahaj, P.A.B. James, IEEE Transactions on Magnetics 29 (1993) 3358–3360.
[22] A.S. Bahaj, P.A.B. James, F.D. Moeschler, IEEE Transactions on Magnetics 32 (1996) 5133–5135.
[23] B. Steinberger, N. Petersen, H. Petermann, D.G. Wiess, Journal of Fluid Mechanics 273 (1994) 189–211.
[24] K. Erglis, Q. Wen, V. Ose, A. Zeltins, A. Sharipo, P.A. Janmey, A. Cebers, Biophysical Journal 93 (2007) 1402–1412.
[25] J.J. Abbott, K.E. Peyer, L. Dong, B. Nelson, The International Journal of Robotics Research 28 (2009) 1434–1447.
[26] W.F. Paxton, K.C. Kistler, C.C. Olmeda, A. Sen, S.K.S. Angelo, Y. Cao, T.E. Mallouk, P.E. Lammert, V.H. Crespi, Journal of the American Chemical Society 126 (2004) 13424–13431.
[27] P. Calvo-Marzal, S. Sattayasamitsathit, S. Balasubramanian, J.R. Windmiller, C. Dao, J. Wang, Chemical Communications 46 (2010) 1623–1624.
[28] W. Wang, S. Li, L. Mair, S. Ahmed, T.J. Huang, T.E. Mallouk, Angewandte Chemie 126 (2014) 3265–3268.

[29] E. Lauga, W.R. DiLuzio, G.M. Whitesides, H.A. Stone, Biophysical Journal 90 (2006) 400–412.
[30] Y. Magariyama, M. Ichiba, K. Nakata, K. Baba, T. Ohtani, S. Kudo, T. Goto, Biophysical Journal 88 (2005) 3648–3658.
[31] S.E.A. Gratton, P.A. Ropp, P.D. Pohlhaus, J.C. Luft, V.J. Madden, M.E. Napier, J.M. DeSimone, Proceedings of the National Academy of Sciences of the United States of America 105 (2008) 11613–11618.
[32] M. Elfar, M. Ayoub, A. Sameh, H. Abass, R.M. Abdel-Kader, I. Gomaa, I.S.M. Khalil, Targeted penetration of MCF-7 cells using iron-oxide nano-particles in vitro, in: Proceedings of the IEEE RAS/EMBS International Conference on Biomedical Robotics and Biomechatronics (BioRob), Singapore, June 2016, pp. 260–265.